



HAL
open science

Towards the development of safer by design TiO₂-based photocatalytic paint: impacts and performances

A. Rosset, V. Bartolomei, J. Laisney, N. Shandilya, H. Voisin, J. Morin, I. Michaud-Soret, Isabelle Capron, H. Wortham, G. Brochard, et al.

► To cite this version:

A. Rosset, V. Bartolomei, J. Laisney, N. Shandilya, H. Voisin, et al.. Towards the development of safer by design TiO₂-based photocatalytic paint: impacts and performances. *Environmental science.Nano*, 2021, 8 (1), pp.758-772. 10.1039/D0EN01232G . cea-03154693

HAL Id: cea-03154693

<https://cea.hal.science/cea-03154693>

Submitted on 1 Mar 2021

HAL is a multi-disciplinary open access archive for the deposit and dissemination of scientific research documents, whether they are published or not. The documents may come from teaching and research institutions in France or abroad, or from public or private research centers.

L'archive ouverte pluridisciplinaire **HAL**, est destinée au dépôt et à la diffusion de documents scientifiques de niveau recherche, publiés ou non, émanant des établissements d'enseignement et de recherche français ou étrangers, des laboratoires publics ou privés.



Cite this: DOI: 10.1039/d0en01232g

Towards the development of safer by design TiO₂-based photocatalytic paint: impacts and performances†

A. Rosset,^{id}*^a V. Bartolomei,^a J. Laisney,^b N. Shandilya,^c H. Voisin,^c J. Morin,^{id}^d I. Michaud-Soret,^{id}^b I. Capron,^{id}^c H. Wortham,^d G. Brochard,^e V. Bergé,^e M. Carriere,^{id}^f F. Dussert,^f O. Le Bihan,^g C. Dutouquet,^g A. Benayad,^a D. Truffier-Boutry,^{id}^a S. Clavaguera^{id}^a and S. Artous^{id}^{*a}

Addition of titanium dioxide (TiO₂) (nano)particles into photocatalytic paints represents a promising alternative aiming to mineralize gaseous pollutants, such as volatile organic compounds (VOCs) into innocuous species (H₂O and CO₂). Despite important industrial and economic benefits, some concerns were raised regarding the risks associated with nano-objects and their human and environmental impacts. To mitigate potential risks associated with the use of these nano-objects, we report a safer by design strategy to develop a photocatalytic paint containing TiO₂ nanoparticles (NPs) taking into consideration the safety aspects over its life cycle. Specific innovative types of TiO₂ NPs were synthesized. These nanoparticles were then incorporated into an organic matrix-based paint. These paints were applied on standard substrates and underwent artificial weathering in an accelerated weathering chamber with controlled parameters. Photocatalytic efficiency towards airborne VOCs was measured for all the paints. Mechanical solicitation through abrasion and incineration tests were performed to assess the potential emission of airborne particles that could lead to human or environmental exposure. In parallel, toxicology studies were conducted to assess the hazards associated with the pristine particles and paint residues. Using this safer by design strategy, we succeeded in decreasing the negative impact of TiO₂ on the paint matrix while keeping a good photocatalytic efficiency and reducing the NP release. Taken together, these results show that we succeeded in generating safer by design paints, thanks to the use of these specifically developed TiO₂ NPs, which exhibit similar photocatalytic properties and enhanced physical properties as compared to paints containing the reference TiO₂ NPs, while reducing their potential hazards.

Received 10th December 2020,
Accepted 7th February 2021

DOI: 10.1039/d0en01232g

rsc.li/es-nano

Environmental significance

Two safer-by-design approaches were investigated to develop specific innovative TiO₂-based photocatalytic paints. The first one was based on titanium nanoparticles' bio-inspired coating. This strategy improved the photocatalytic activity compared to a classical paint and allowed a reduction of nano-TiO₂ release into the environment. The second one was based on titanium nanoparticles' grafting onto CNC. This approach allowed the reduction of nano-titanium quantity incorporated into the paint for an equivalent photocatalytic activity to a classical paint. The results confirm the potential of adding TiO₂ NPs into paints for air purification with a lower release into the environment throughout the whole life cycle of paints.

^a CEA, LITEN, DTNM, LMSE, Univ. Grenoble Alpes, F-38000 Grenoble, France.

E-mail: aurelie.rosset0868@gmail.com, sebastien.artous@cea.fr

^b CEA, CNRS, BIG, CBM, Univ. Grenoble Alpes, F-38000 Grenoble, France

^c INRAE, UR BIA, F-44316, Nantes, France

^d CNRS, LCE, UMR 7376, Aix Marseille Université, 13331 Marseille, France

^e ALLIOS, Les Docks II, 185 Chemin de Saint-Lambert, F-13821 La Penne-sur-Huveaune, France

^f CEA, CNRS, INAC, SYMMES, Univ. Grenoble Alpes, F-38000 Grenoble, France

^g Institut National de l'Environnement Industriel et des Risques (INERIS), Parc Technologique Alata BP 2, 60550 Verneuil-en-Halatte, France

† Electronic supplementary information (ESI) available. See DOI: 10.1039/d0en01232g

Introduction

Improving air quality is becoming an important concern for human health and climate. Volatile organic compounds (VOCs), nitrogen oxides (NO_x), carbon monoxide (CO), sulfur dioxide (SO₂) and fine particles, as organic and inorganic air pollutants, can have an impact on health. The World Health Organization (WHO) reports that indoor air pollution accounts for an estimated 4.2 million deaths per year due to stroke, heart disease, lung cancer and chronic respiratory diseases.¹

In order to remove these pollutants, active and passive filtration systems are used. Passive filtration systems adsorb through physisorption or chemisorption VOCs on the surface of porous materials (*e.g.* activated carbon, zeolite).^{2,3} However, the main problems of these technologies lie on their selectivity to certain VOCs and the additional disposal or handling steps. Active filtration systems are based on photocatalytic oxidation,⁴ plasma processes⁵ and ozone generation,⁶ which aims at mineralizing VOCs. Photocatalytic oxidation induces the mineralization of VOCs by producing radical species thanks to photo-excitation of a solid catalyst under irradiation. Compared to other techniques, photocatalytic oxidation is a cost-effective and environmentally friendly technology that uses a renewable energy source, involves little maintenance, and can be easily implemented. The main drawback of this technology is the potential generation of harmful by-products.

Photocatalytic oxidation is a promising air purification technique which allows the mineralization of VOCs into innocuous species (H_2O and CO_2) at room temperature. During the last few decades, TiO_2 has become one of the most attractive photocatalysts, in particular due to its strong oxidizing capacity, its chemical stability and its affordability.^{7,8} On this basis, TiO_2 has been studied extensively for VOC degradation.^{9,10} More recently, TiO_2 was modified through several techniques producing doped TiO_2 , surface modified TiO_2 , mesoporous TiO_2 , semiconductor coupled TiO_2 and supported TiO_2 in order to enhance VOC degradation efficiency.^{11–14}

To improve air quality, it was found that the application of TiO_2 based paint onto the outdoor and indoor covering of buildings may be a good complement to conventional technologies.^{15–18} In particular, TiO_2 is currently incorporated in building materials to degrade VOCs such as xylene, benzene, toluene, formaldehyde and benzo-[a]-pyrene.^{18–24} When incorporated in photocatalytic paints, its efficiency for VOC degradation has been quantified by Truffier-Boutry *et al.*, using xylene as a test compound.²⁵ The degradation kinetics of this gaseous compound by a paint surface containing TiO_2 NPs was 60 times faster than that of a paint surface without TiO_2 NPs. Moreover, Salthammer *et al.* showed efficient degradation of formaldehyde by a photocatalytic wall paint.²⁶ In parallel, some studies showed that photocatalytic paints might release VOCs and TiO_2 NPs into the environment. It was shown that the emitted VOCs came from the photocatalytic degradation of the organic matrix of the paint.^{15,25,27} On the other hand, as shown by Shandilya *et al.*, free TiO_2 NPs were emitted during artificial weathering in air and lixiviats.²⁸ Fiorentino *et al.* investigated the release of NPs from different paint formulations before and after several types of aging.²⁹ They showed that the paint formulation containing SiO_2 NPs and TiO_2 pigment did not release free NPs but fragments of the paint matrix containing these particles. Al-Kattan *et al.* reported that paints containing TiO_2 NPs released TiO_2 as leachate during climatic weathering.³⁰ All these studies have focused on

increasing the photocatalytic efficiency of these paints. We conducted an innovative approach in a safer by design concept³¹ through the development of new formulations to reduce the amount of TiO_2 nanoparticles or to coat them while keeping good photocatalytic efficiency. The aim is to decrease their release from the paint when subjected to weathering or/and mechanical solicitation. The proposed approach relies on the conception, the synthesis and the implementation of TiO_2 supported photocatalytic sites in next generation paints. To achieve this objective, the present study aimed at developing a paint containing photocatalytic, safer by design TiO_2 NPs following the strategy described in Fig. 1.

The safer by design strategy consisted of: (i) engineering the chemical surface of TiO_2 NPs to avoid TiO_2 and VOC release induced by the degradation of the matrix of paints and (ii) functionalization of TiO_2 NPs to reduce the TiO_2 quantity in the paint. For that, new photocatalytic TiO_2 NPs were synthesized following two different routes. The first one consists of coating commercial TiO_2 NPs with bio-inspired ligands (route 1) and the second one consists of grafting TiO_2 NPs onto cellulose nanocrystals (CNC) forming TiO_2 -CNC hybrids (route 2). Some of these newly synthesized NPs, TiO_2 NPs were coated with PEG3350, PAA, and DOPA (route 1) and TiO_2 -CNC hybrids included at 0.5%_{wt}, 0.72%_{wt}, 0.9%_{wt} and 1.32%_{wt} (route 2), were then incorporated into an organic matrix-based paint. The paints were applied on standard Leneta and Taber substrates, then underwent artificial weathering and were analyzed by means of scanning electron microscopy (SEM), X-ray photoelectron spectroscopy (XPS) and energy dispersive X-ray spectroscopy (EDX) along the different steps.

In addition, the photocatalytic efficiency of the paints was studied to evaluate their ability to degrade VOCs (*i.e.* *m*-xylene). Moreover, mechanical solicitation (*i.e.* abrasion) was performed and the subsequent emission of airborne particles was monitored. In addition, incineration tests were performed. Using sampling on transmission electron microscope (TEM) grids, the morphologies and elemental compositions of the aerosol particles and the residue were examined. In parallel, toxicology studies were conducted in order to assess the hazards of pristine particles and paint residues collected after abrasion tests.

Materials and methods

Chemicals for TiO_2 nanoparticles coated with bio-inspired ligands (route 1)

Commercial TiO_2 NPs were provided by the paint manufacturer ALLIOS (France). Polyethylene glycol (PEG, molar weight of 3350 g mol^{-1}), poly(acrylic acid) (PAA, molar weight of 1800 g mol^{-1}), 3,4-dihydroxy-L-phenylalanine (DOPA, purity $\geq 98\%$), disodium pyrophosphate ($\text{Na}_2\text{H}_2\text{P}_2\text{O}_7$, purity $\geq 99\%$) and tetrasodium pyrophosphate ($\text{Na}_4\text{P}_2\text{O}_7$, purity $\geq 95\%$) were all purchased from Sigma Aldrich.

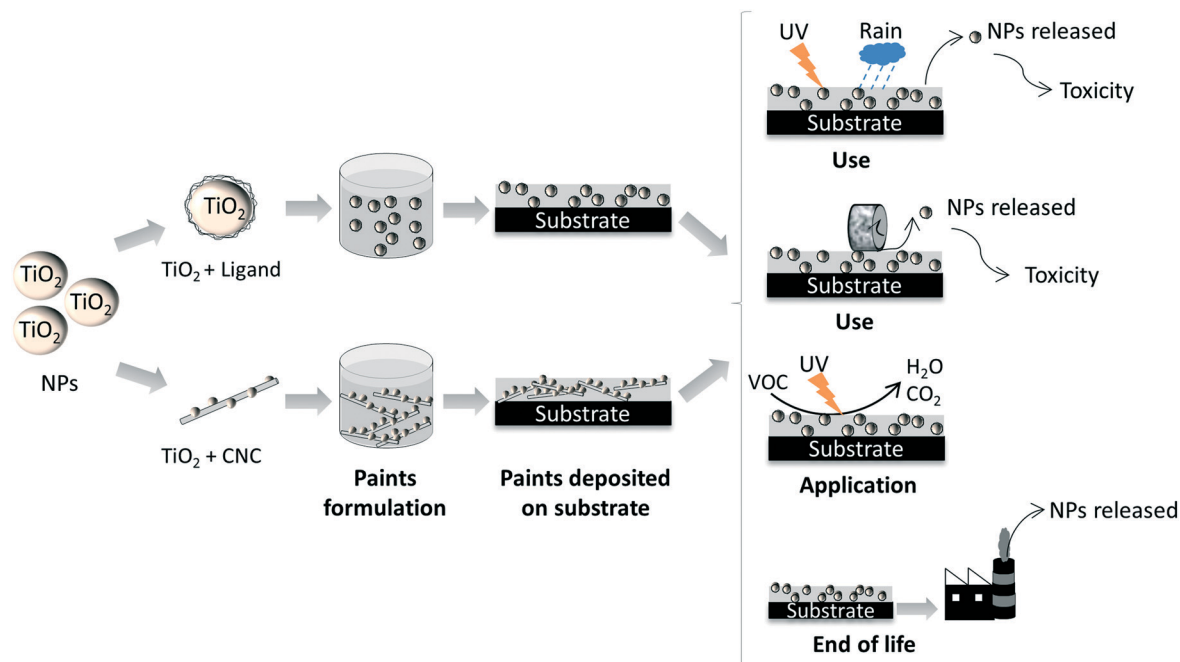


Fig. 1 Schematic presentation of safer by design approaches for TiO₂ based photocatalytic paints.

Chemicals for TiO₂ nanoparticles grafted onto CNC (route 2)

CNC were provided by the Process Development Center at the University of Maine, received as a 12.2%_wt suspension in water. Sulfuric acid (H₂SO₄, analytical grade, purity >95%) was purchased from Fisher Scientific and TiOSO₄ (15%_wt in dilute sulfuric acid solution) was purchased from Sigma-Aldrich.

TiO₂ nanoparticle synthesis and coating

New types of photocatalytic TiO₂ NPs were synthesized following the two aforementioned synthesis approaches.

Route 1: commercial TiO₂ NPs were coated with bio-inspired polymers (PEG and PAA) and a molecule (DOPA) following a titanium in surface (Ti_{surf})/ligand molar ratio of 1/1 according to the formula.³² After dispersion in a pyrophosphate buffer medium by 1 hour sonication (pulse 1 s on/1 s off, 80% amplitude) at a concentration of 10 mg mL⁻¹, the suspensions of TiO₂ NPs were added dropwise to a solution of the ligand and mixed for 1 hour at 60 °C in a reactor (Omni station OS1025, Electrothermal, Fisher Scientific, UK). Coated particles were then collected by centrifugation at 1000 rpm for 10 minutes and washed twice with water in order to remove the ligand not attached to the TiO₂ NP surface. Then, the pellet was either dispersed in pyrophosphate buffer to ensure maximal dispersion conditions during the formulation of the paints or dried at 50 °C in an oven for morphological and chemical characterization.

Route 2: TiO₂ NPs grafted onto cellulose nanocrystals (CNC) were synthesized by a sol-gel process. First, the CNC suspension diluted to 5 g L⁻¹ was sonicated (15 minutes at

approx. 25 W). H₂SO₄ was added to the suspension to a concentration of 0.1 M, then TiOSO₄ to a concentration of 4.5 mM. The mixture was stirred for 2 hours and 45 minutes at room temperature. The resulting suspension was purified by repeated centrifugation (20 000g, 20 minutes) and washed with distilled water to remove all non-fixed TiO₂ NPs. The sample appeared as a white coloured precipitate composed of TiO₂-CNC hybrid nanostructures.

Paint formulation

These TiO₂ NPs synthesized were incorporated into an organic matrix-based paint by the manufacturer ALLIOS (France). As classically formulated in the paint industry, the organic-based paint was composed of acrylic, microsized TiO₂ providing the white colour (pigment), calcium carbonate particles, aluminosilicate, water and other additives. The microsized TiO₂ particles have a mean particle size distribution (PSD) of primary particles of 240 nm (Fig. S1†). The newly synthesized TiO₂ NPs were incorporated in this paint, *i.e.* commercial TiO₂ NPs (P2), commercial TiO₂ NPs coated with bio-inspired ligands (P3, P4 and P5) or TiO₂ NPs grafted onto CNC (P6, P7, P8 and P9) as reported in Table 1. According to the safer by design strategy, the amount of TiO₂ NPs in paints was selected in order to maintain the paint stability and keep a good photocatalytic activity. These eight paints were applied on standard Taber (aluminum, Taber industries, USA) and Leneta (black plastic-vinyl chloride/acetate copolymer with a smooth matt surface, Leneta company, USA) substrates by a manual film applicator, obtaining a wet thickness of 100 μm and 150 μm, respectively.

Table 1 Compositions of the reference paint, paints containing commercial TiO₂ NPs coated with bio-inspired ligands (route 1) and paints based on TiO₂ NPs grafted onto CNC (route 2)

	Name	Nanoparticles	Amount of microsized TiO ₂ (wt%)	Amount of TiO ₂ NPs (wt%)
Reference paint	P2	Commercial TiO ₂ NPs	10.0	3.5
Paints containing TiO ₂ NPs coated with bio-inspired ligands	P3	Commercial TiO ₂ NPs + PEG3350 (polyethylene glycol) with [PEG3350]/[Ti] ratio = 1/1	10.0	3.5
	P4	Commercial TiO ₂ NPs + PAA (poly(acrylic acid)) with [PAA]/[Ti] ratio = 1/1	10.0	3.5
	P5	Commercial TiO ₂ NPs + DOPA (3,4-dihydroxy-L-phenylalanine) with [DOPA]/[Ti] ratio = 1/1	10.0	3.5
Paints containing TiO ₂ NPs grafted onto CNC	P6	TiO ₂ + 0.5% _{wt} CNC	10.0	0.13
	P7	TiO ₂ + 0.72% _{wt} CNC	10.0	0.19
	P8	TiO ₂ + 0.9% _{wt} CNC	10.0	0.23
	P9	TiO ₂ + 1.32% _{wt} CNC	10.0	0.35

Artificial weathering: Q-UV climatic chamber

Leneta and Taber substrates coated with these paint formulations were subjected to artificial weathering in an accelerated weathering chamber (model QUV accelerated weathering, Q-Lab, USA), according to the ISO 16474-3 standard. The paints were exposed to UVB-313 lamps for 5 hours under the following conditions: an irradiance of 0.71 W m⁻² at 310 nm, temperature set at 50 ± 3 °C and a relative humidity of 50%. A second step was applied for 1 hour under wet conditions where water was sprayed at a flow rate of 7 L min⁻¹ to reach a specific relative humidity of 100% and a temperature of 25 ± 3 °C without irradiation. The paints underwent sequentially those cycles for 500 hours and 1000 hours.

Mechanical solicitation: abrasion testing

A standard wear resistance test was applied on the paints deposited on Taber substrates before and after artificial weathering. This test consisted of mechanical solicitation by abrasion performed on a Taber rotary abraser (model Abraser 5135, Taber industries, USA), according to the ISO 7784-2 standard. It was done with two sets of CS-0 type wheels covered with S42 abrasive sticker paper at a load of 500 g for a rotation speed of 60 rpm for 200 cycles. The particles released by the abrasion process were characterized in real time in terms of PSD and concentration using respectively a fast mobility particle sizer (FMPS, model 3091, TSI Incorporated, USA) and a condensation particle counter (CPC, model 3775, TSI Incorporated, USA). The FMPS allowed measurement of aerosol particles ranging from 5.6 nm to 560 nm. The CPC counts airborne particles ranging from 5 nm to 3 µm in diameter. In addition, a collection device installed on a sampling rod allowed the released particles to be trapped on a hydrophilic polycarbonate membrane (pore size 0.4 µm, Millipore, USA). The collected samples were characterized by SEM-EDX to determine the particle morphology, size and elemental chemical composition. The experiments were performed in a 0.25 m³ glove box equipped with a HEPA filter reducing the particle concentration

background below 5 particles per cm³. The glove box air was extracted upwards (HEPA filter at the bottom and extraction at the top) at a rate of 150 L min⁻¹.

Photocatalytic efficiency

The photocatalytic efficiency of the paints was experimentally measured to compare the ability of the paints containing TiO₂ NPs to improve indoor air quality, which represents restrictive photocatalytic conditions. For this purpose, two experiments were carried out: the first one to quantify the VOC elimination capacity of the photocatalytic paints using *m*-xylene as a model compound and the second one to determine the VOC emission fluxes induced by the degradation of the matrix of the paints under UV-vis irradiation. For the first experiment, paints deposited on Leneta substrates were exposed to UV-vis irradiation in a thermostated double-wall flow tube photo-reactor equipped with a movable injector to vary the paint surface area exposed to *m*-xylene.^{33,34} The experimental set up with more details such as *m*-xylene generation and PTR-MS conditions is shown in Fig. S2 and Text. S1.†

Briefly, the flow tube irradiation device was composed of six lamps (Philips TL-D 18 W Actinic BL, 340–400 nm, λ_{max} = 368 nm, length = 60 cm) simulating UV solar irradiation. The flow tube was made of borosilicate glass with an internal volume of 131 cm³. A sheath flow (200 mL min⁻¹) was fed to a humidification system before its introduction in the reactor. Downstream the flow tube, a hygrometer (HYGROLOG-HL-NT2, Rotonic, France) with a probe (HygroClip SC04) measured on-line the resulting humidity with ±1.5% RH accuracy. Furthermore, the photo-reactor was coupled to a proton transfer reaction mass spectrometer (PTR-MS, Ionic-on AnalytikGmbH, Austria) for on-line and continuous measurements of VOC concentrations. The experimental conditions were as follows: pressure of synthetic air (Linde gas, France, >99.999 stated purity) of 1 atm, light intensity of 8.8 W m⁻², temperature of 25 °C, relative humidity of 40% and 50 ppb *m*-xylene concentration upstream the reactor. For each experiment, four different

Table 2 Distance to the end of reactor, exposed paint surface and contact time between paint and gaseous *m*-xylene as a function of movable injector position

Position	Distance (cm)	Exposed surface (cm ²)	Contact time (s)
A ₀	0	0	0
A ₁	4	7.6	5.4
A ₂	8	15.2	10.9
A ₃	15	28.5	20.4
A ₄	22	41.8	29.9

positions were carried out. The distance to the end of the reactor, residence time and photocatalytic area are described in Table 2.

Kinetic measurements

One of the aims of this work was to determine the photocatalytic efficiency of the different photocatalytic paints. In this case, the kinetic constant was calculated. It is a pseudo-first order rate constant (k) of *m*-xylene loss (s⁻¹). k was determined by the slope of $\ln(C_0/C_x)$ plotted as a function of the residence time (t) (Table 2). C_0 is the initial concentration of gaseous *m*-xylene in position A₀ (end of the reactor). C_x is the concentration at different positions from A₁ to A₄. The difference in concentration between A₀ and A_x corresponds to the amount of *m*-xylene consumed on the paint surface by the photocatalytic effect. After each position change, the injector was pushed into the initial position to go back to the initial conditions. The variation of the concentration as a function of residence time enabled the kinetic constant to be calculated. A typical experiment for paint P3 after 1000 hours of exposure to artificial weathering is shown in Fig. S3 and S4.†

Incineration

The incineration experimental setup was presented in detail in previous works.³⁵ The furnace is 150 cm long with an inner diameter of 95 mm. The dry residues of paints were scratched on Taber substrates and introduced in an Inconel-made meshed holder (diameter of 30 mm and 25 mm height). The sample holder was meshed so as to let the air flow in to facilitate the combustion. When incinerating the samples, the sample holder was pushed through the furnace centre to ensure incineration of its content. Dry air was flowed through the furnace with a flow rate of 12 L min⁻¹. The flow rate was set to ensure fully oxidative combustion in incineration mode. The accurate conditions that were defined to ensure proper incineration are indicated hereafter. The inner furnace temperature was set to 850 °C, and a residence time of two seconds in the post-combustion zone was ensured. Turbulence conditions were met in the furnace so that a good mix between combustible gases and oxygen and a high excess of oxygen concentration were reached. These four rules are usually applied in incinerator plants. Several instruments were implemented to monitor gas and

particulate emissions. A gas analyzer (Horiba PG350, Japan) allowed the monitoring of the temporal evolutions of the O₂, CO₂ and CO concentrations. The combustion phases could therefore be identified by monitoring the temporal evolution of these gases. A particle sizer (DMS500 Cambustion, UK) was used for real-time particulate emission monitoring. It allowed the determination of particle size distributions and concentrations for sizes ranging from a few nanometers to 1 μm. Airborne particles were sampled using a mini particle sampler (MPS, Ecomesure, France) on a TEM grid.³⁶ Collected particles were characterized by TEM. For each sample studied, the measurements were repeated three times. For each measurement, a sample mass of around 100 mg was introduced in the Inconel-made meshed holder. The MPS grids were sampled with a time duration of 15 s. The sampling started the moment the holder was pushed through the furnace. The residue of the combustion (what is left after combustion) was analyzed with TEM.

Toxicology study

Toxicity evaluation was performed on the A549 cell line, which are human alveolar epithelial cells, because the most probable exposure route to these NPs is *via* inhalation of paint residues. These cells were purchased from the European Collection of Authenticated Cell Cultures (ECACC) (reference: 86012804). They were grown in DMEM-glutamax containing 4.5 g L⁻¹ glucose and supplemented with 10% fetal bovine serum, 50 U mL⁻¹ penicillin and 50 μg mL⁻¹ streptomycin, at 37 °C and 5% CO₂. For toxicity experiments, cells were seeded in 96 well plates at a density of 62 500 cells per cm² (WST1) or 15 000 cells per cm² (53BP1).

NPs were diluted in complete cell culture medium to the final concentrations of 6.25, 12.5, 25, 50, 100 μg mL⁻¹ (WST1) or 50 μg mL⁻¹ (53BP1). Polystyrene-amine NPs (PS-NH₂, 100 μg mL⁻¹) and etoposide (100 μM) were used as the positive control in the WST1 assay and 53BP1 assay, respectively.

The cytotoxicity of commercial TiO₂ NPs, commercial TiO₂ NPs + PEG3350, TiO₂ + 0.5%_wt CNC and paint residues collected after abrasion tests (P2, P3 and P6 for commercial TiO₂ NPs, commercial TiO₂ NPs + PEG3350 and TiO₂ + 0.5%_wt CNC, respectively) was evaluated using the WST1 assay (Roche), which probes the cell metabolic activity. Briefly, after 24 hours of exposure to the particles, the exposure medium was replaced with 100 μL of WST1 solution diluted to the tenth in FBS-free cell culture medium. After 90 minutes of incubation at 37 °C, the absorbance was measured at 450 nm, probing the appearance of formazan, and corrected by background absorbance at 650 nm.

The genotoxicity of particles was evaluated using 53BP1 immunolabelling, 53BP1 being involved in the complex of DNA double strand break repair.³⁷ After 24 hours of exposure to particles, cells were fixed with 4% paraformaldehyde and permeabilized with 0.2% triton X-100 prepared in PBS containing 3% BSA (washing buffer). Cells were then rinsed

three times with washing buffer and exposed to anti-53BP1 primary antibody (Abnova, PAB12506, dilution 1/500) for 1 hour at room temperature under mild agitation. Cells were then rinsed three times for 5 minutes with washing buffer and exposed to anti-rabbit IgG-Atto488 secondary antibody (Sigma Aldrich, 18772, dilution 1/2000), for 1 hour at room temperature under mild agitation. They were finally washed three times with washing buffer, counterstained with 5 $\mu\text{g mL}^{-1}$ Hoechst 33342 for 15 minutes at room temperature, then washed three times with PBS and stored until analysis. Automatic counting of 53BP1 foci in cell nuclei was performed on a CellInsight CX5 high content screening platform.

Both assays were repeated three times independently, with 5 replicates per condition in each independent experiment. Statistical analysis consisted of Kruskal–Wallis ANOVA, followed when statistically significant by paired comparison using the Mann–Whitney test (Statistica version 7.1, Statsoft). Results were considered statistically significant when p was lower than 0.05.

Characterization over the whole life cycle

The BET surface area measurement was carried out on commercial TiO_2 NPs by N_2 sorption at 77 K on a BELSORP-max instrument (Japan). The sample was previously outgassed at 400 °C for 1000 minutes under secondary vacuum. The surface morphology of synthesized NPs and paints deposited on Leneta substrates before and after artificial weathering as well as on the aerosolized particles collected during the abrasion process was investigated by scanning electron microscopy (SEM-FEG, LEO 1530, Germany). All the samples were coated with a 10 nm thick platinum layer deposited by sputtering. Images were acquired with a working distance of 4 mm, an accelerating voltage of 5 kV, a magnification of $\times 100\text{k}$ and a diaphragm aperture of 30 μm .

The presence of coating on the TiO_2 surface was confirmed by Fourier-transformed infrared spectroscopy (FTIR, Spectrum 100 Optica Perkin Elmer spectrometer, USA). FTIR spectra were collected in the 2100–500 cm^{-1} range, with 1 mg of powder and 99 mg of KBr and a resolution of 4 cm^{-1} at room temperature.

The elemental chemical composition of the aerosolized particles collected during abrasion was analyzed by energy dispersive X-ray spectroscopy (EDX, QUANTAS EDS, Bruker Nano assisted software ESPRIT, USA) in the SEM. The working distance of the samples and accelerating voltage were respectively raised to 8 mm and 15 kV. A diaphragm aperture of 60 μm was used.

For TiO_2 –CNC hybrid visualization, a transmission electron microscope (TEM, JEOL JEM-1230, USA) was employed at an accelerating voltage of 40 kV. Before their microscopy analyses, the samples were prepared by depositing $\approx 20 \mu\text{l}$ of a 10-fold diluted dispersion onto a glow discharged carbon-coated electron microscope grid (200

mesh, Delta Microscopies, France) for 2 minutes. Excess solution was removed by blotting. The crystalline structure of TiO_2 NPs in the hybrid was validated by X-ray diffraction (XRD, Bruker D8 Discover diffractometer, USA). Spectra were recorded every 10 minutes. Cu-K α radiation ($\lambda = 1.5406 \text{ \AA}$), produced in a sealed tube at 40 kV and 40 mA, was selected and parallelized using a Göbel mirror parallel optics system and collimated to produce a 500 mm beam diameter. The fraction of TiO_2 NPs in the hybrid was measured by thermogravimetric analysis on a TGA 2050 of TA Instruments, France. The temperature was varied in the range of 25 °C to 900 °C by using a Platinel II $\text{\textcircled{R}}$ thermocouple (Engelhard Industries). The heating rate was kept at 10 °C min^{-1} . To obtain Fourier-transformed infrared (FTIR) spectra, a Thermo Scientific Nicolet IS50 spectrometer was operated in transmission mode between 4000 and 400 cm^{-1} . 2 mg of powder was ground with 120 mg of KBr and compressed to obtain a thin pellet. Each FTIR spectrum was averaged automatically by the spectrometer over 200 scans.

The chemical composition of paints applied on Leneta substrates before and after artificial weathering was analyzed by X-ray photoelectron spectroscopy (XPS, Versaprobe II ULVAC-PHI spectrometer, Japan) with an Al K α monochromatic X-ray source of 100 μm diameter. Survey (0–1200 eV) and high-resolution (C 1s, O 1s and Ti 2p) spectra were recorded. The atomic percentage of surface elements was determined from the high-resolution spectra using ULVAC-PHI Multipack software, with respect to the photoelectron sensibility factors per atom and orbital. The binding energy position of spectra was calibrated from the carbon C 1s peak at 285 eV corresponding to the alkyl groups of PMMA.

The morphology and size of aerosolized particles collected during incineration and ashes were analyzed using a transmission electron microscope (TEM, JEOL JEM 1400 Plus, Japan). The possibilities offered by such an instrument include imagery (morphology, size) and elemental analysis of large areas of the grid integrating several particles or of single particles (minimum size of 10 nm) using the energy dispersive X-ray spectroscopy (EDX, Oxford assisted software Oxford AZTEC, UK) technique. For the ashes, TEM analysis required preparation. The solid residue was put in a mixture of alcohol and water and sonicated in an ultrasonic bath. Then a drop of the solution was deposited on the TEM grid after plasma treatment and dried prior to analysis.

Results and discussion

Characterization of synthesized TiO_2 nanoparticles

The commercial TiO_2 NPs were in anatase form (Fig. S5 \dagger) with a mean particles size distribution (PSD) of primary particles of 7.2 nm (Fig. S6 \dagger). The BET surface area of these TiO_2 NPs was evaluated to be 214.3 $\text{m}^2 \text{g}^{-1}$ and their N_2 adsorption–desorption isotherm is shown in Fig. S7 \dagger . The morphology and presence of coating around TiO_2 NPs were investigated by SEM as shown in Fig. 2a. The pristine

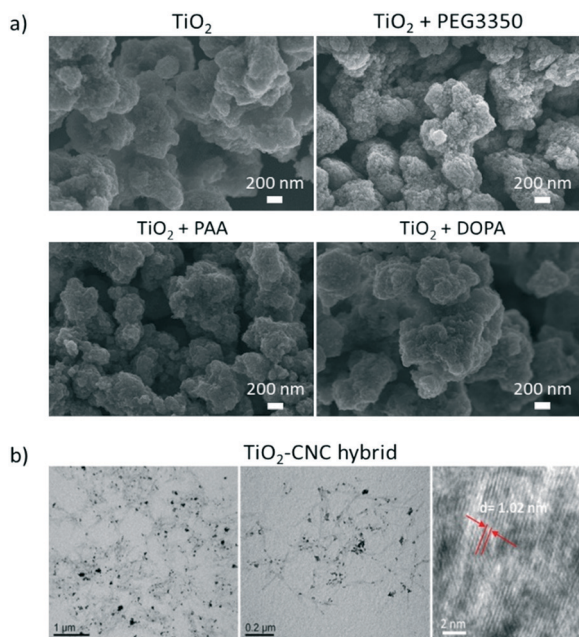


Fig. 2 (a) SEM images of pristine commercial TiO₂ NPs and commercial TiO₂ NPs coated with bio-inspired ligands: PEG3350, PAA and DOPA and (b) TEM images of TiO₂-CNC hybrid nanostructures at 2 magnifications (left and middle) and HRTEM image of one of the nucleated TiO₂ NPs showing the anatase crystal planes (right).

commercial TiO₂ is depicted in Fig. 2a as well as the TiO₂ NPs coated with PEG3350, TiO₂ NPs coated with PAA and TiO₂ NPs coated with DOPA. The materials bearing various coatings were composed of agglomerated spherical NPs in the micrometer range. The surface roughness of TiO₂ NPs coated with PEG3350 was greater than that of pristine commercial TiO₂ NPs while TiO₂ NPs coated with PAA and DOPA look the same. The presence of ligands on the surface was confirmed by FTIR spectroscopy (Fig. S8†) with additional vibration bands observed in the spectra of the TiO₂ coated NPs compared to the uncoated NPs and assigned to different ligand functional groups.³⁸

TEM was used in order to define the repartition of TiO₂ along the TiO₂-CNC hybrid nanostructures. In Fig. 2b, nanorod structures with lengths varying from 150 nm to 300 nm can be observed with darker structures representing the TiO₂ NPs. Further magnification shows that the TiO₂ NPs are well grafted onto the CNC. When one of these black points was analyzed using HRTEM (Fig. 2b), we observed well-defined crystalline structures with a fringe spacing of 1.02 nm that represents the interplane distance in the anatase phase.

Such an image illustrates that the hybrids prepared appear as isolated nanorods bearing TiO₂ NPs on their surface.

The anatase form of TiO₂ NPs was validated by X-ray diffraction (XRD) with a peak appearing at 25° (JCPDS, no. 21-1272) (and no visible peak at 27.5°, JCPDS, no. 21-1272, where the rutile form is visible) as shown in Fig. S9†. The fraction of TiO₂ in the hybrid of 26%_w was determined by thermogravimetry (Fig. S10†). The presence of TiO₂ NPs

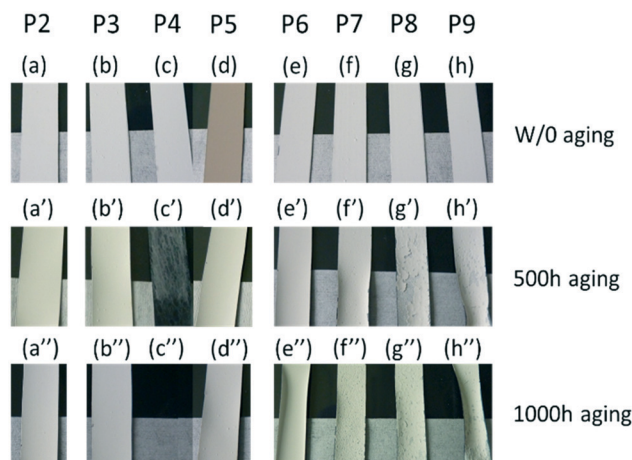


Fig. 3 Photograph of paints P2, P3, P4 and P5, respectively (a)–(d), and paints P6, P7, P8 and P9, respectively (e)–(h), before and after 500 hours (noted with (')) and 1000 hours (noted with ('')) of exposure to artificial weathering. The change in colour is an artefact from the photographs and paints before and after artificial weathering are white at sight.

grafted onto CNC was confirmed by FTIR spectroscopy (Fig. S11†).

Characterization of the paint surfaces before and after ageing

Images of the paint surfaces deposited on Leneta substrates before and after artificial weathering are shown in Fig. 3. Before artificial weathering, a colour modification of paint surfaces was observed depending on the paint formulation. One can notice a change in colour from white to brown throughout the addition of TiO₂ NPs coated with DOPA into the paint (P5, Fig. 3d). This coloration comes from the ligand-to-metal charge transfer (LMCT) band after the covalent grafting of DOPA on the TiO₂ NP surface. After exposure to artificial weathering conditions, different modifications at the paint surface were noticeable. For paint P5, the surface became white after artificial weathering (Fig. 3d' and d'') which could be explained by the progressive degradation of the DOPA coating during artificial weathering. For paints P4, P7, P8 and P9, a degradation of the paint surface was observed after artificial weathering as shown in Fig. 3c', c'', f', f'', g', g'', h' and h''. In contrast, Fig. 3a', a'', b', b'', e' and e'' did not show any degradation of paints P2, P3 and P6. The surface of these paints remained white without crackling after artificial weathering. This shows that addition of TiO₂ NPs coated with PEG3350 and TiO₂ grafted onto CNC at a concentration of 0.5%_w into the paints ensured a good stability of the paint on the substrate. These two paints remained stable even after artificial weathering. Paint P5 was abandoned because it did not correspond to the current specifications of a commercial photocatalytic paint, which included white colour.

The surface of the paints deposited on Leneta substrates was then characterized by SEM in order to study the artificial

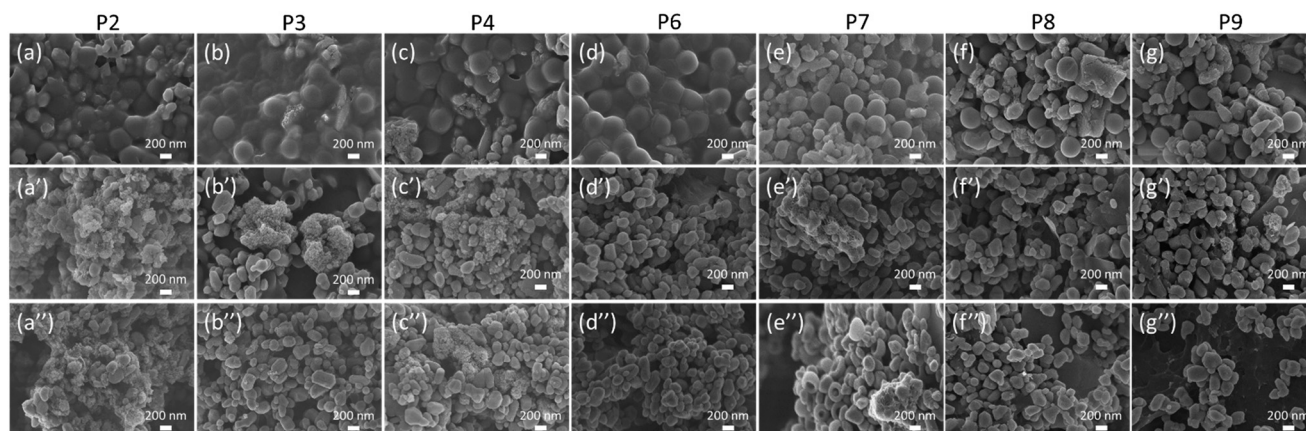


Fig. 4 SEM images of paints P2, P3, P4, P6, P7, P8 and P9, respectively, before artificial weathering (a)–(g), after 500 hours of exposure (a')–(g') and after 1000 hours of exposure (a'')–(g'').

weathering impact on the material morphologies. Fig. 4 compares the SEM images of paints P2, P3, P4, P6, P7, P8 and P9 (Fig. 4a–g, respectively) before and after 500 hours (noted with (')) and 1000 hours (noted with ('')) of exposure to artificial weathering. All the SEM images show that the particles incorporated into the paints before artificial exposure were partially covered by a thin organic matrix layer. For paints P2 and P4 after 500 hours (Fig. 4a' and c') and 1000 hours of exposure (Fig. 4a'' and c''), this organic matrix was not visible anymore.

However, the organic matrix was observed at the paint surface of P3 after 500 hours but not after 1000 hours of exposure (Fig. 4b' and b'', respectively). For paints P6, P7, P8 and P9, the organic matrix was observed after both 500 hours and 1000 hours of artificial weathering. The number of particles (paint constituents) covered by an organic matrix all along artificial weathering indicates the surface degradation state.

As a conclusion, the organic matrix present partially at the surface of paints P2, P3, P6, P7, P8 and P9 was degraded with artificial weathering. This degradation leads to an increase of particles on the paint surface. The paint surface becomes porous after artificial weathering. These porosities lead to an increase of the active surface and improves accessibility to catalytic sites and thus the contact between TiO_2 and air. This effect was previously reported in the literature for the paint with SiO_2 or TiO_2 NPs after UV exposure.^{25,29}

To go deeper in the understanding of the organic matrix degradation due to artificial weathering, the paint surfaces deposited on Leneta substrates before and after artificial weathering were investigated by XPS. According to the photographs and SEM results presented above, only stable paints with an organic matrix partially on their surfaces such as paints P2, P3 and P6 were studied. The high-resolution XPS spectra of C 1s, O 1s and Ti 2p regions of these paints are presented in Fig. 5. The C 1s spectra are fitted with peaks at 284.8 eV, 286.3 eV, 289 eV and 290.1 eV binding energies attributed to C–C/C–H, C–O, COO and CO_3 , respectively. The first three peaks have been attributed to the organic matrix

and CO_3 was identified and attributed to the CaCO_3 used in the paint formulation.³⁹ For paint P6 (Fig. 5g), a supplementary peak appears at 289.3 eV. This peak was identified and attributed to Na_2CO_3 .⁴⁰ The oxygen O 1s peak was composed of three peaks at 531 eV, 532.4 eV and 533 eV, which were assigned to O^{2-} , C=O and C–O (Fig. 5b, e and h). The C=O bonding was attributed to the acrylic and vinyl copolymers used in the paint formulation. The titanium Ti 2p peak was associated with Ti $2p_{3/2}$ and Ti $2p_{1/2}$ at 458.6 eV and 464.3 eV, respectively. The difference in energy between these two peaks was 5.7 eV. This is specific of the spin-orbit coupling of the Ti^{4+} oxidation state of titanium in the TiO_2 form. It can be seen in the spectra of paint P2 before (in red in Fig. 5a–c) and after artificial weathering (500 hours of exposure in blue and 1000 hours of exposure in green in

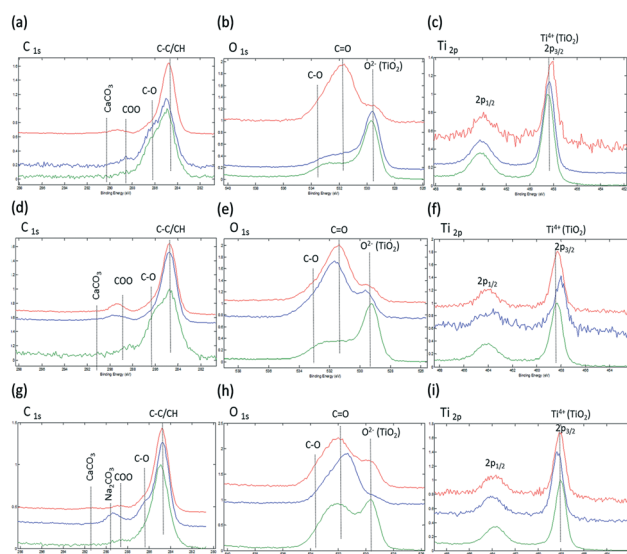


Fig. 5 XPS spectra of paints P2, P3 and P6 before artificial weathering (in red), after 500 hours of exposure (in blue) and after 1000 hours of exposure (in green). C 1s (a), O 1s (b) and Ti 2p (c) spectra of paint P2, C 1s (d), O 1s (e) and Ti 2p (f) spectra of paint P3 and C 1s (g), O 1s (h) and Ti 2p (i) spectra of paint P6.

Fig. 5a–c) that the intensity of the C–O and C–C/CH peaks decreases while the O²⁻ peak increases as a result of artificial weathering. Moreover, the C=O O 1s related peak intensity decreased after artificial weathering between 0 and 500 hours and remained stable. These indicate that the organic matrix of paint P2 after artificial weathering was degraded. This degradation leads to an increase of TiO₂ NPs on the paint surface. This is also supported by the atomic concentration as summarized in Table S1,[†] where the carbon decreased from 82.4%.at to 30.5%.at and the titanium increased from 1.8%.at to 22.1%.at after 1000 hours. In the case of paint P3, the C=O peak evolves mainly after 500 hours of exposure to artificial weathering. This result is corroborated in the frame of the C 1s peak; the COO related peak decreases while the C–O related one increases. These results might find origin in the photocatalytic process induced by the electronic exchange between photoactivated electrons between the TiO₂ valence band and conduction band and the LUMO level of PEG molecules.^{41–43} This phenomenon induces polymer decomposition, as evidenced by the enhancement of the Ti 2p peak intensity (O²⁻ (TiO₂) peak intensity). Since the depth of analysis in XPS is ~10 nm, and in the frame of thin film approximation, it seems that the thickness of the polymer film covering the TiO₂ particles is reduced. This result corroborates the observation discussed in the frame of SEM analyses (Fig. 4). The atomic concentration of paint P3 is shown in Table S2.[†] However, a shift of the Ti 2p_{3/2} peak toward lower binding energies is observed in Fig. 5f between paint P3 before artificial weathering and after 500 hours of exposure to artificial weathering. This can be attributed to a change in the chemical extreme surface composition of TiO₂ particles that leads to a dipole surface modification. Thus, the Ti⁴⁺ formal oxidation state of titanium is not modified. However, the chemical environment probed with the titanium atoms would appear to be modified. In the case of paint P6 after and before artificial weathering, the situation is similar in some aspects such as the intensity of the C–O and C–C/CH peaks related to C 1s decreases slightly and the O²⁻ peak increases slightly. As summarized in Table S3,[†] the carbon slightly decreased after 1000 hours. This indicates that the organic matrix is more resistant to UV and leaching, leading to a more durable paint. However, the TiO₂–CNC connection at the atomistic level indicates that the catalytic process is different. For instance, the mean free path of the induced photocatalytic electrons does not react with the accessible LUMO level of CNC.⁴¹ Thus, XPS analysis confirms that increasing the artificial weathering time induced a higher degradation of the organic matrix and consequently an accumulation of TiO₂ NPs on the paint surface, which could be released eventually as airborne particles upon mechanical solicitation. This is also in agreement with the SEM images shown in Fig. 4. Chiantore *et al.* showed that acrylate copolymer paint was degraded under UV-light exposure.⁴⁴ They attributed this effect to a photo-oxidative removal of the acrylate copolymer, *via* chain scission and/or volatilization of organic fragments during artificial

weathering. This degradation induced an increase in the surface concentration of inorganic species. The increasing amount of inorganic species, *i.e.*, TiO₂ and SiO₂ at the paint's surface after artificial weathering was also observed by several authors.^{29,45,46} The coating of TiO₂ NPs with PEG3350 and grafting of TiO₂ NPs onto CNC decreased the degradation of the organic matrix-based paint compared to the pristine TiO₂ NPs. The organic matrix of paint P6 presented the best result against artificial weathering.

Abrasion induced airborne particle emission

The particle size distribution and the particle number concentration were monitored in real time using respectively an FMPS and a CPC during the abrasion process of paints deposited on Taber substrates before and after artificial weathering. The particle number concentration from FMPS and CPC instruments is represented in Fig. 6 and S12.[†] The total concentration of particles released measured by the FMPS was greater than the one measured by the CPC. Some studies report that above 200 nm particle size, the particle number concentration is overestimated by the FMPS as compared to other instruments.⁴⁷ The paints after artificial weathering were more prone to release particles than the original samples. This is related to a degradation of the organic matrix paint during artificial weathering as shown in SEM images (Fig. 4) and XPS spectra (Fig. 5). Moreover, not surprisingly, particle emission increased when the artificial weathering time increased from 500 hours to 1000 hours, except for paint P6. The airborne particle emission in the nanometer range (≤100 nm) from paints P3 and P6 was 1.2 and 1.5 times lower than that from paint P2. The same trend was observed on the emitted submicron and micro-sized fractions. The particle size distribution from the FMPS of paints is reported in Fig. S13.[†] It shows that the modal diameter of particles released from paint P3 is around 140 nm while those of particles released from paints P2 and P6 are less than 100 nm. Paints P3 and P6 before and after

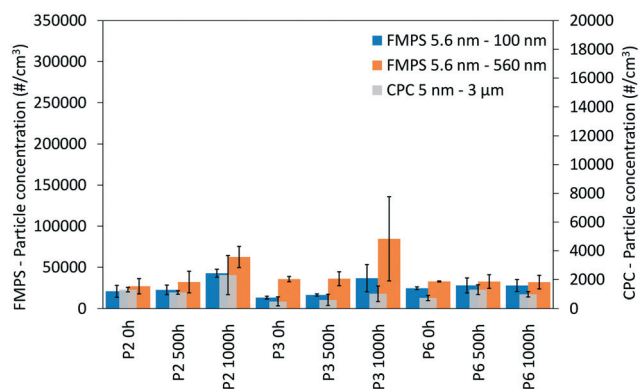


Fig. 6 Concentration of particles released per cm³ before and after artificial weathering as a function of the particle size measured with an FMPS (left scale) in blue from 5.6 nm to 100 nm and in orange from 5.6 nm to 560 nm and a CPC (right scale) in grey from 5 nm to 3 μm.

artificial weathering were the least emissive in terms of aerosol resulting from abrasion tests in comparison to the reference paint P2. As compared to our previous study,²⁵ the organic matrix-based paint with only TiO₂ pigment before and after UV irradiation presents a lower particle number concentration emitted than the paint containing TiO₂ NPs after UV irradiation. In other words, adding TiO₂ NPs into the paint formulation leads to an increase of particles released.

In order to go further in the analysis of the airborne released particles during the abrasion process, they were collected on a hydrophilic polycarbonate membrane and characterized by SEM to determine their size and morphology. Fig. 7 compares only the SEM images of membranes for the reference paint P2 (Fig. 7a, a' and a'') and the least emissive paints P3 (Fig. 7b, b' and b'') and P6 (Fig. 7c, c' and c'') before and after artificial weathering. They show that the mainly emitted agglomerates are micrometric with size ranging from 1 to 4 μm. In addition, the presence of low amounts of submicron agglomerates with size ranging from 100 to 600 nm and individual NPs with size ranging from 20 to 100 nm was observed for paint P2 in Fig. 8 and paints P3 and P6 in Fig. S14† at a higher magnification. The shape and size of aerosols released during the abrasion process did not change regardless of artificial weathering.

In order to further investigate the abrasion tests conducted on the different paints, additional EDX analysis was performed. The EDX spectra obtained for the particles released from paints P2, P3 and P6 before and after artificial weathering are shown in Fig. S15.† EDX analysis shows that, whatever the paint, the micrometric agglomerates (Fig. 7) were composed of carbon, oxygen, aluminum, silicon, calcium and titanium, as well as platinum coming from the coating, which corresponds to paint fragments. The individual particles with submicron size and individual NPs as shown in Fig. 8 and in Fig. S14† were composed of carbon,

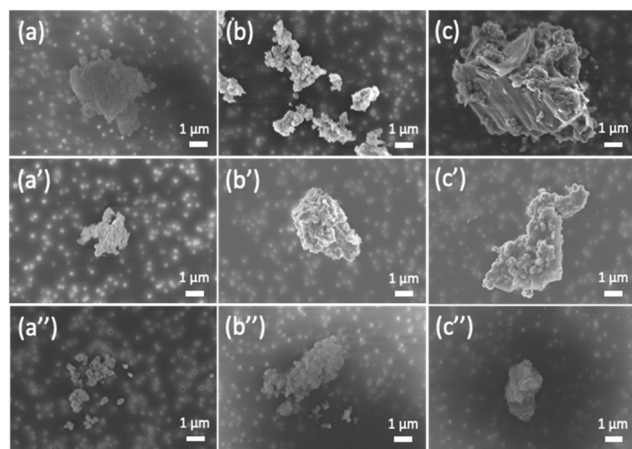


Fig. 7 SEM images of particles released from paints P2, P3 and P6 respectively before artificial weathering (a)–(c), after 500 hours of exposure (a')–(c') and after 1000 hours of exposure (a'')–(c'').

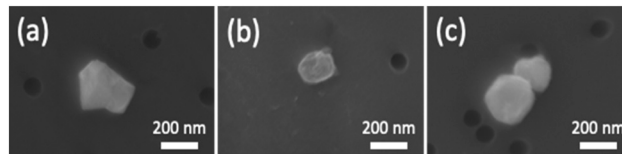


Fig. 8 SEM images of submicron agglomerates, individual submicron particles, and individual NPs released from paint P2 before artificial weathering (a), after 500 hours of exposure (b) and after 1000 hours of exposure of (c).

oxygen, titanium and platinum (Fig. S16†), which corresponds to TiO₂. The origin of those TiO₂ particles cannot be discriminated between the micrometric TiO₂ pigment and the nanometric TiO₂ catalyst added to the paint formulation. Consequently, the aerosols released from paints P2, P3 and P6 during abrasion were composed of both individual TiO₂ particles and TiO₂ particles still embedded in the organic matrix. Shandilya *et al.* also showed that the individual TiO₂ NPs can be released into air by abrasion of building materials with TiO₂ after artificial weathering.²⁸ However, numerous studies show that the large fraction of the emitted NPs is linked to the matrix and is not alone.^{29,48–51} As XPS analysis shows, stepwise and complete organic matrix degradation of paints leaves on the surface a larger amount of TiO₂ particles that can be released over time. Therefore, the accumulated TiO₂ particles at the paint's surface were released during the abrasion process.

Consequently, adding TiO₂ NPs coated with PEG3350 and grafted onto CNC at a concentration of 0.5%_{wt} into paints decreased the degradation of the binder and avoided the important release of NPs. Furthermore, the abrasion data confirm that increasing artificial weathering leads to degradation of the organic matrix and to increased release of particles in air. This result complements our previous surface analysis of the paints. Using a safer by design approach it was found that paints P3 and P6 are promising in terms of stability over time.

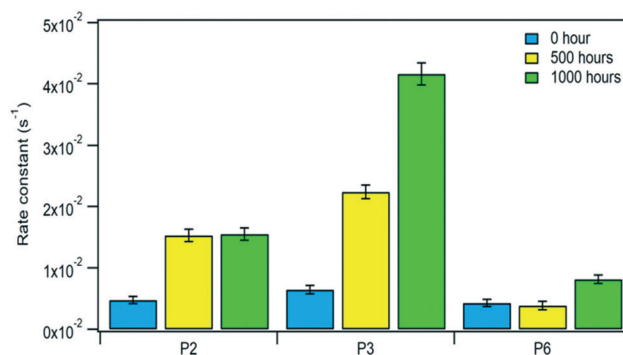


Fig. 9 *m*-Xylene kinetic constant as a function of paints P2, P3 and P6 before and after artificial weathering for 500 hours and 1000 hours. The errors bars are derived from uncertainties associated with experiments.

Photocatalytic efficiency

The kinetic constants measured for *m*-xylene photocatalytic degradation are representative of paints' efficiency to eliminate VOCs from indoor atmospheres. The experimental results are reported in Fig. 9 for paints P2, P3, and P6 and in Fig. S17† for paints P4, P5, P7, P8 and P9 deposited on Leneta substrates before and after artificial weathering. The values are reported in Table S4.† Before artificial weathering, the photocatalytic efficiencies of seven of the eight paints were in the same order of magnitude; only paint P3 showed a significantly higher kinetic constant. The kinetic constants of paints P6 to P9 raised progressively as the amount of TiO₂ NPs grafted onto CNC increased, thus demonstrating the influence of TiO₂ concentration on the photocatalytic efficiency. However, these results show also that an adapted design of TiO₂ NPs can increase the photocatalytic efficiencies since the nano-TiO₂ concentration embedded in the reference paint (P2) was 10.3 times higher than in paint P9 for a similar photocatalytic efficiency. After artificial weathering, the photocatalytic efficiencies of paints P2, P3 and P5 raised drastically (up to a factor 3.6, 6.4 and 4.8, respectively) and this increase was generally correlated with the weathering duration. To facilitate the comparison, the removal efficiency (RE) in position A₄ had been calculated for the different paints (Tables 3 and S5†).

As shown in our previous study,²⁵ the organic matrix-based paints with TiO₂ pigment and without TiO₂ NPs (control tests) before and after UV irradiation are not photocatalytic, whereas the paint containing TiO₂ NPs degrades xylene after UV irradiation. In agreement with SEM observations and XPS analysis, these results suggest that the increase of the photocatalytic efficiency is correlated to the degradation of the organic paint matrix. Indeed, in the paints before artificial weathering a significant fraction of TiO₂ NPs is embedded which makes them less efficient for VOC degradation since there is less access for VOCs to TiO₂ NPs, while in the paints after artificial weathering, TiO₂ NPs were released from the matrix gangue and became accessible and thus active for VOC degradation. As a result, the design of TiO₂ NPs grafted onto CNC seems promising, because it avoids the degradation of the paint by matrix elimination and allows the reduction of nanoparticle concentration while keeping the photocatalytic efficiency stable overtime. The efficiency of paints with bio-inspired ligand coated NPs suggests that paint P3 could be interesting because the amount of NPs inside the paint could be decreased by at least

a factor of two for the same efficiency as paint P2. Moreover, a previous study has shown that the organic matrix-based paint has a total emission of VOCs 43% higher than a mineral matrix-based paint.⁵² The mineral matrix seems to be a key factor in the development of paints to improve air quality.

End of life

Based on the safer by design strategy and as shown in previous results, paints P2, P3 and P6 before artificial weathering were selected. Thus, dry residues of these paints were scratched on Taber substrates and incinerated to assess whether nanometric-sized TiO₂ could be released either in the aerosol and/or found in the ashes. For each sample, the aerosol and ashes were examined using TEM and analysed using EDX. First, global analyses were performed on areas of 60 μm × 60 μm, then individual particles were analysed.

Aerosolized particle characterization during incineration

For the aerosol emitted from paints P2 and P3 before artificial weathering, the global EDX analysis showed the presence of calcium, silicon, aluminum, magnesium and

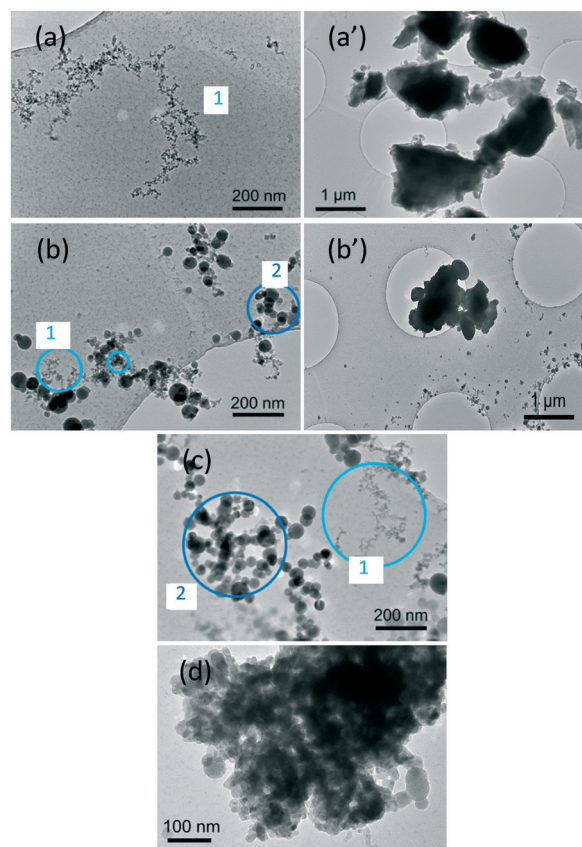


Fig. 10 TEM images of nanostructured particles of carbonaceous soot found in the aerosol when incinerating paint P2 (a), particles found in the aerosol when incinerating paints P2 (a'), P3 (b) and P6 (c), micrometric-sized particle of TiO₂ (b') and nanostructured particles of TiO₂ (d) found in the aerosol when incinerating paint P3.

Table 3 Removal efficiency of *m*-xylene in position A₄ for photocatalytic paints P2, P3 and P6 before and after artificial weathering for 500 hours and 1000 hours

Paints	RE	RE	RE
	0 hour (%)	500 hours (%)	1000 hours (%)
P2	10.9	38.5	44.5
P3	13.5	41.5	68.4
P6	13.2	16.4	21.3

oxygen, which are the basic elements of the organic matrix-based paint. These aerosols were composed of both nanostructured particles (Fig. 10a and b) and micrometric-sized agglomerates (Fig. 10a' and b) which correspond to carbonaceous soot and paint fragments, respectively. In the aerosols from incinerated paint P2, no titanium was detected, contrary to the aerosols from incinerated paint P3. In this sample, in addition to the latter two categories of particles, micrometric-sized aggregates (Fig. 10b') as well as a few number of nanostructured particles (Fig. 10d) composed of titanium and oxygen were detected. These nanostructured TiO₂ particles are probably the nanometric TiO₂ catalyst added to the paint formulation. Therefore, TiO₂ was released as agglomerates from paint P3. Regarding the aerosols resulting from the incineration of paint P6, the particles were mainly composed of silicon, aluminum, carbon, oxygen and sodium (Fig. 10c). They showed both spherical particles composed of aluminum and oxygen with size of 30–100 nm and agglomerates of nanometric-sized particles composed of silicon, carbon and oxygen. Titanium was not found in this aerosol. As a conclusion, TiO₂ is not found in the aerosols from incinerated paints P2 and P6 before artificial weathering.

Ash characterization after incineration

The global EDX analysis showed that the calcium, titanium and oxygen elements dominate the elemental composition of all the ashes, whatever the paint (P2, P3 and P6). Moreover, small quantities of silicon were also found in these ashes. Aluminum and magnesium were also found in small quantities in the ashes of paints P2 and P6 and paint P3, respectively. Two categories of particles were observed (Fig. 11): (i) particles with size >100 nm composed of calcium, titanium and oxygen, in relative abundances suggesting that they could be calcium titanate (CaTiO₃), as previously observed by Massari *et al.*,⁵³ and (ii) nanometric-sized particulates composed of calcium and oxygen suggesting that they could be calcium oxide. There could be also micrometric-sized particles of TiO₂ coming from the pigment present in the paints. This suggests interestingly that TiO₂ is not found in nanometric form in the ashes.

Effect of the paint residues on cytotoxicity and genotoxicity

The cytotoxicity and genotoxicity of these particles, either pristine or paint residues collected after abrasion tests, were

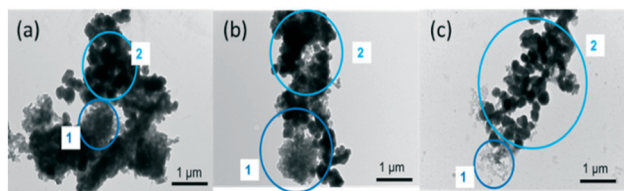


Fig. 11 Particles found in the ashes when incinerating paints P2 (a), P3 (b) and P6 (c) before artificial weathering.

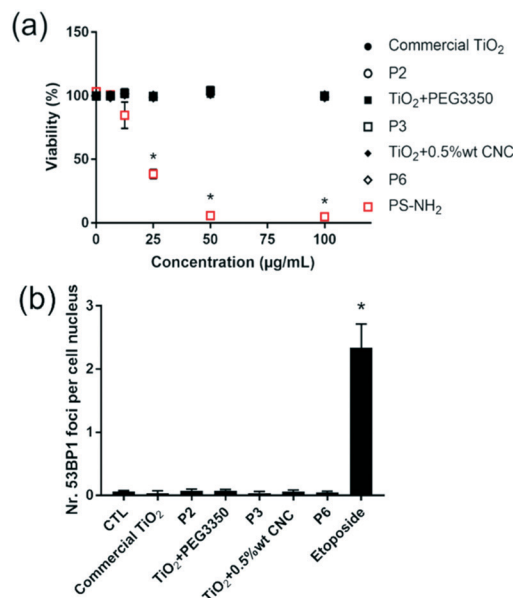


Fig. 12 Cyto- and genotoxicity of TiO₂ NPs and paint residues. Cytotoxicity was assessed via the WST1 assay on A549 cells exposed for 24 hours to 0–100 μg mL⁻¹ particles, either pristine (commercial TiO₂ NPs, commercial TiO₂ NPs + PEG3350, and TiO₂ + 0.5%wt CNC) or paint residues collected after abrasion tests (P2, P3 and P6 for commercial TiO₂ NPs, commercial TiO₂ NPs + PEG3350, and TiO₂ + 0.5%wt CNC, respectively). Polystyrene-amine (PS-NH₂, 100 μg mL⁻¹) was used as a positive control in the cytotoxicity assay (a). Genotoxicity was assessed by counting the number of 53BP1 foci in the nucleus of A549 cells exposed for 24 hours to 50 μg mL⁻¹ of these particles. Etoposide (100 μM) was used as a positive control (b). Statistical significance: **p* < 0.05, exposed vs. CTL, Mann–Whitney test.

assessed on A549 lung epithelial cells. Cell viability, as assessed via the WST1 assay, which measures cell metabolic activity, did not decrease significantly after exposure to these particles, proving that these particles were not cytotoxic, upon exposure up to 100 μg mL⁻¹ for 24 hours (Fig. 12a). Neither did they induce any elevation of the number of 53BP1 foci, reflective of DNA strand breaks, *i.e.* of the genotoxicity of the particles (Fig. 12b). Therefore, all these particles were considered safe to A549 cells under our exposure conditions, which constitute a worst case scenario as the concentrations used here are more than 10⁶-fold higher than human inhalation exposure under extreme conditions.⁵⁴

Conclusions

Safer by design strategies were implemented for the development of innovative photocatalytic paints by synthesizing new nanoTiO₂-based catalysts. This strategy involves a reduction of the amount of TiO₂ NPs incorporated in the paints or the incorporation of self-protecting TiO₂ NPs for given photocatalytic properties and thus, a lower release of TiO₂ NPs into the environment throughout the whole life cycle of paints. Therefore, TiO₂ NPs coated with PEG3350, PAA, and DOPA and TiO₂ NPs grafted onto CNC at a

concentration of 0.5%_{w/w}, 0.72%_{w/w}, 0.9%_{w/w} and 1.32%_{w/w} were synthesized by two different approaches. These synthesized NPs were then incorporated into an organic matrix based photocatalytic paint. The photocatalytic results before artificial weathering showed that paint P3 (commercial TiO₂ NPs coated with PEG3350) enhances the photocatalytic efficiency, whereas for paint P6 (TiO₂ grafted onto CNC at a concentration of 0.5%_{w/w}), the photocatalytic efficiency remains the same as the reference paint P2. However, paint P6 incorporates a lower amount of TiO₂ NPs in weight content than the two other paints. The photocatalytic efficiency of paint P3 increased after artificial weathering. Paint P3 exhibits excellent photocatalytic efficiencies with a low level of particle emission in comparison to the reference paint P2 in terms of the amount of photocatalytic NPs added into each paint.

Characterization of paints using XPS demonstrates that carbon, corresponding to the organic matrix, was degraded by 46.4% after 500 hours of exposure to artificial weathering for P3, whereas it was only 24.7% after 1000 hours for P6. In contrast, the degradation of the organic matrix of paint P2 was observed between 0 and 500 hours of exposure to artificial weathering. Besides this observation, paints P3 and P6 were the least emissive in terms of aerosol resulting from abrasion tests. The results lead to the conclusion that UV degradation and leaching of the organic matrix increase the accumulation of TiO₂ NPs at the surface of the paint that can be released as airborne particles during mechanical solicitation. This observation is coherent with a previously described aging mechanisms also known as chalking. The modification and functionalization of TiO₂ NPs improve the durability of the paints towards artificial weathering. Toxicology tests show that the paint residues were not cytotoxic. Moreover, the aerosols generated by paints P2 and P6 before artificial weathering during incineration were found to be free of the titanium element. In contrast, titanium was found in the aerosol when incinerating paint P3 before artificial weathering. It was observed that there were micrometric-sized aggregates and nanostructured particles (their number was quite low) both made of TiO₂. However, in the residue, it should be noted that TiO₂ NPs were not found when incinerating whatever paint before artificial weathering. EDX analysis suggests that these are made of calcium oxide.

By taking into account the reduction of TiO₂ concentration inside the paint and the NPs released while keeping a good photocatalytic efficiency, paints P3 and P6 appear to be the most promising candidates. These results confirm the potential of adding TiO₂ NPs into paints for air purification but require a fine-tuning of several parameters of the paint formulation such as the matrix, as it was shown that the mineral matrix-based paint is the least VOC emitter compared to the organic matrix counterpart. The authors are currently investigating the influence of this mineral matrix using the best candidates of the safer by design specifically developed nanocomposites described in the present study,

i.e. the TiO₂ NPs coated with PEG3350, using a lower concentration and the TiO₂ NPs grafted onto CNC at a concentration of 0.5%_{w/w}, introduced in a mineral matrix-based paint. The properties of those new paints will have to be again fully characterized throughout their life cycle. The present work developed here in the context of photocatalytic paint innovation for air depollution demonstrates all the prospects of a safer by design approach integrated throughout the life cycle of the active product.

Conflicts of interest

There are no conflicts to declare.

Acknowledgements

The authors acknowledge Dominique Locatelli, Arnaud Guiot and Olivier Sicardy from CEA for their respective help with the SEM-EDX analysis, abrasion tests and XRD analysis and Cynthia Oueiny for fruitful discussion. We also thank Olivier Aguerre-Chariol and Laurent Meunier from INERIS for their help during incineration experiments. This work is a contribution to the LABEX SERENADE (no. ANR-11-LABX-0064) funded by the "Investissements d'Avenir" French Government program of the French National Research Agency (ANR) through the A*MIDEX project (No. ANR-11-IDEX-0001-02).

References

- 1 Who, *Ambient air pollution: Health impacts*, Dep. Public Heal. Environ. Soc. Determ. Heal., 2016.
- 2 J. Pei and J. S. Zhang, Determination of adsorption isotherm and diffusion coefficient of toluene on activated carbon at low concentrations, *Build. Environ.*, 2012, **48**, 66–76.
- 3 K. J. Kim and H. G. Ahn, The effect of pore structure of zeolite on the adsorption of VOCs and their desorption properties by microwave heating, *Microporous Mesoporous Mater.*, 2012, **152**, 78–83.
- 4 D. Vildozo, R. Portela, C. Ferronato and J. M. Chovelon, Photocatalytic oxidation of 2-propanol/toluene binary mixtures at indoor air concentration levels, *Appl. Catal., B*, 2011, **107**, 347–354.
- 5 M. Ragazzi, P. Tosi, E. C. Rada, V. Torretta and M. Schiavon, Effluents from MBT plants: Plasma techniques for the treatment of VOCs, *Waste Manage.*, 2014, **34**, 2400–2406.
- 6 H. F. Hubbard, B. K. Coleman, G. Sarwar and R. L. Corsi, Effects of an ozone-generating air purifier on indoor secondary particles in three residential dwellings, *Indoor Air*, 2005, **15**, 432–444.
- 7 A. Fujishima and X. Zhang, Titanium dioxide photocatalysis: present situation and future approaches, *C. R. Chim.*, 2006, **9**, 750–760.
- 8 F. van Broekhuizen and J. C. van Broekhuizen, *Nanotechnology in the European Construction Industry-State of the art 2009- Executive Summary*, Eur. Fed. Build. Wood Work, Amsterdam, Netherlands, 2009, pp. 1–30.

- 9 N. Quici, M. L. Vera, H. Choi, G. L. Puma, D. D. Dionysiou, M. I. Litter and H. Destailats, Effect of key parameters on the photocatalytic oxidation of toluene at low concentrations in air under 254 + 185 nm UV irradiation, *Appl. Catal., B*, 2010, **95**, 312–319.
- 10 A. Nakajima, H. Obata, Y. Kameshima and K. Okada, Photocatalytic destruction of gaseous toluene by sulfated TiO₂ powder, *Catal. Commun.*, 2005, **6**, 716–720.
- 11 H. Sun, S. Wang, H. M. Ang, M. O. Tadé and Q. Li, Halogen element modified titanium dioxide for visible light photocatalysis, *Chem. Eng. J.*, 2010, **162**, 437–447.
- 12 H. Ichiura, T. Kitaoka and H. Tanaka, Removal of indoor pollutants under UV irradiation by a composite TiO₂-zeolite sheet prepared using a papermaking technique, *Chemosphere*, 2003, **50**, 79–83.
- 13 Z. Shayegan, C. S. Lee and F. Haghighat, TiO₂ photocatalyst for removal of volatile organic compounds in gas phase – A review, *Chem. Eng. J.*, 2018, **334**, 2408–2439.
- 14 S. S. Nair, J. Chen, A. Slabon and A. P. Mathew, Converting cellulose nanocrystals into photocatalysts by functionalisation with titanium dioxide nanorods and gold nanocrystals, *RSC Adv.*, 2020, **10**, 37374–37381.
- 15 A. Gandolfo, S. Marque, B. Temime-Roussel, R. Gemayel, H. Wortham, D. Truffier-Boutry, V. Bartolomei and S. Gligorovski, Unexpectedly High Levels of Organic Compounds Released by Indoor Photocatalytic Paints, *Environ. Sci. Technol.*, 2018, **52**, 11328–11337.
- 16 A. Dianatdar and M. Jamshidi, Investigation of inter-relationship between tensile behavior and photocatalytic activity of an acrylic-based composite upon UVA exposure, *J. Appl. Polym. Sci.*, 2017, **134**, 1–9.
- 17 T. Maggos, J. G. Bartzis, P. Leva and D. Kotzias, Application of photocatalytic technology for NO_x removal, *Appl. Phys. A: Mater. Sci. Process.*, 2007, **89**, 81–84.
- 18 A. Basso, A. P. Battisti, R. de F. P. M. Moreira and H. J. José, Photocatalytic effect of addition of TiO₂ to acrylic-based paint for passive toluene degradation*, *Environ. Technol.*, 2020, **41**, 1568–1579.
- 19 A. Strini, S. Cassese and L. Schiavi, Measurement of benzene, toluene, ethylbenzene and o-xylene gas phase photodegradation by titanium dioxide dispersed in cementitious materials using a mixed flow reactor, *Appl. Catal., B*, 2005, **61**, 90–97.
- 20 J. Chen, C. sun Poon, Photocatalytic construction and building materials: From fundamentals to applications, *Build. Environ.*, 2009, **44**, 1899–1906.
- 21 J. Gunschera, J. R. Andersen, N. Schulz and T. Salthammer, Surface-catalysed reactions on pollutant-removing building products for indoor use, *Chemosphere*, 2009, **75**, 476–482.
- 22 H. Taoda, M. Fukaya, E. Watanabe and K. Tanaka, VOC Decomposition by Photocatalytic Wall Paper, *Mater. Sci. Forum*, 2006, **510–511**, 22–25.
- 23 J. Auvinen and L. Wirtanen, The influence of photocatalytic interior paints on indoor air quality, *Atmos. Environ.*, 2008, **42**, 4101–4112.
- 24 B. Tryba, P. Homa, R. J. Wróbel and A. W. Morawski, Photocatalytic decomposition of benzo-[a]-pyrene on the surface of acrylic, latex and mineral paints. Influence of paint composition, *J. Photochem. Photobiol., A*, 2014, **286**, 10–15.
- 25 D. Truffier-Boutry, B. Fiorentino, V. Bartolomei, R. Soulas, O. Sicardy, A. Benayad, J. F. Damlencourt, B. Pépin-Donat, C. Lombard, A. Gandolfo, H. Wortham, G. Brochard, A. Audemard, L. Porcar, G. Gebel and S. Gligorovski, Characterization of photocatalytic paints: A relationship between the photocatalytic properties-release of nanoparticles and volatile organic compounds, *Environ. Sci.: Nano*, 2017, **4**, 1998–2009.
- 26 T. Salthammer and F. Fuhrmann, Photocatalytic surface reactions on indoor wall paint, *Environ. Sci. Technol.*, 2007, **41**, 6573–6578.
- 27 O. Geiss, C. Cacho, J. Barrero-Moreno and D. Kotzias, Photocatalytic degradation of organic paint constituents-formation of carbonyls, *Build. Environ.*, 2012, **48**, 107–112.
- 28 N. Shandilya, O. Le Bihan, C. Bressot and M. Morgeneyer, Emission of Titanium Dioxide Nanoparticles from Building Materials to the Environment by Wear and Weather, *Environ. Sci. Technol.*, 2015, **49**, 2163–2170.
- 29 B. Fiorentino, L. Golanski, A. Guiot, J.-F. Damlencourt and D. Boutry, Influence of paints formulations on nanoparticles release during their life cycle, *J. Nanopart. Res.*, 2015, **17**, 149.
- 30 A. Al-Kattan, A. Wichser, R. Vonbank, S. Brunner, A. Ulrich, S. Zuin and B. Nowack, Release of TiO₂ from paints containing pigment-TiO₂ or nano-TiO₂ by weathering, *Environ. Sci.: Processes Impacts*, 2013, **15**, 2186–2193.
- 31 J. Y. Bottero, J. Rose, C. De Garidel, A. Masion, T. Deutsch, G. Brochard, M. Carrière, N. Gontard, H. Wortham, T. Rabilloud, B. Salles, M. Dubosson, B. Cathala, D. Boutry, A. Ereskovsky, C. Auplat, L. Charlet, T. Heulin, E. Frejafon and S. Lanone, SERENADE: safer and ecodesign research and education applied to nanomaterial development, the new generation of materials safer by design, *Environ. Sci.: Nano*, 2017, **4**, 526–538.
- 32 I. A. Janković, Z. V. Šaponjić, E. S. Džunuzović and J. M. Nedeljković, New Hybrid Properties of TiO₂ Nanoparticles Surface Modified With Catecholate Type Ligands, *Nanoscale Res. Lett.*, 2010, **5**, 81–88.
- 33 A. Gandolfo, V. Bartolomei, E. Gomez Alvarez, S. Tlili, S. Gligorovski, J. Kleffmann and H. Wortham, The effectiveness of indoor photocatalytic paints on NO_x and HONO levels, *Appl. Catal., B*, 2015, **166–167**, 84–90.
- 34 L. I. Nieto-Gligorovski, S. Gligorovski, S. Tlili, X. Fu, B. Temime-Roussel and H. Wortham, An Approach to Determine Isopropanol Sorption Kinetics on Wafers by Reactor Coupled to Proton Transfer Reaction Mass Spectrometry, *J. Electrochem. Soc.*, 2009, **156**, H290.
- 35 G. Ounoughene, O. Le Bihan, C. Chivas-Joly, C. Motzkus, C. Longuet, B. Debray, A. Joubert, L. Le Coq and J. M. Lopez-Cuesta, Behavior and fate of halloysite nanotubes (HNTs) when incinerating pa6/HNTs nanocomposite, *Environ. Sci. Technol.*, 2015, **49**, 5450–5457.

- 36 B. R'Mili, O. L. C. Le Bihan, C. Dutouquet, O. Aguerre-Chariol and E. Frejafon, Particle sampling by TEM grid filtration, *Aerosol Sci. Technol.*, 2013, **47**, 767–775.
- 37 L. Anderson, C. Henderson and Y. Adachi, Phosphorylation and Rapid Relocalization of 53BP1 to Nuclear Foci upon DNA Damage, *Mol. Cell. Biol.*, 2001, **21**, 1719–1729.
- 38 J. Laisney, A. Rosset, V. Bartolomei, D. Predoi, D. Truffier-Boutry, S. Artous, V. Bergé, G. Brochard and I. Michaud-Soret, TiO₂ nanoparticles coated with bio-inspired ligands for the safer-by-design development of photocatalytic paints, *Environ. Sci.: Nano*, 2021, **8**, 297–310.
- 39 S. L. Stipp and M. F. Hochella Jr, Structure and bonding at the calcite surface as observed with X-ray photoelectron spectroscopy (XPS) and (LEED), *Geochim. Cosmochim. Acta*, 1991, **55**, 1723–1736.
- 40 A. V. Shchukarev and D. V. Korolkov, XPS study of group IA carbonates, *Cent. Eur. J. Chem.*, 2004, **2**, 347–362.
- 41 S. Li, S. Xu, L. He, F. Xu, Y. Wang and L. Zhang, Photocatalytic Degradation of Polyethylene Plastic with Polypyrrole/TiO₂ Nanocomposite as Photocatalyst, *Polym.-Plast. Technol. Eng.*, 2010, **49**, 400–406.
- 42 J. F. Rabek, *Polymer Photodegradation*, 1995.
- 43 C. H. Hare, The Degradation of Coatings by Ultraviolet Light and Electromagnetic Radiation, *J. Prot. Coat. Linings*, 1992, 8029–8032.
- 44 O. Chiantore and M. Lazzari, Photo-oxidative stability of paraloid acrylic protective polymers, *Polymer*, 2001, **42**, 17–27.
- 45 T. Nguyen, B. Pellegrin, C. Bernard, X. Gu, J. M. Gorham, P. Stutzman, D. Stanley, A. Shapiro, E. Byrd, R. Hettenhouser and J. Chin, Fate of nanoparticles during life cycle of polymer nanocomposites, *J. Phys.: Conf. Ser.*, 2011, **304**, 012060.
- 46 J. M. Gorham, T. Nguyen, C. Bernard, D. Stanley and R. David Holbrook, Photo-induced surface transformations of silica nanocomposites, *Surf. Interface Anal.*, 2012, **44**, 1572–1581.
- 47 M. Levin, A. Gudmundsson, J. H. Pagels, M. Fierz, K. Møllhave, J. Löndahl, K. A. Jensen and I. K. Koponen, Limitations in the Use of Unipolar Charging for Electrical Mobility Sizing Instruments: A Study of the Fast Mobility Particle Sizer, *Aerosol Sci. Technol.*, 2015, **49**, 556–565.
- 48 M. Vorbau, L. Hillemann and M. Stintz, Method for the characterization of the abrasion induced nanoparticle release into air from surface coatings, *J. Aerosol Sci.*, 2009, **40**, 209–217.
- 49 C. Bressot, N. Manier, C. Pagnoux, O. Aguerre-Chariol and M. Morgeneyer, Environmental release of engineered nanomaterials from commercial tiles under standardized abrasion conditions, *J. Hazard. Mater.*, 2017, **322**, 276–283.
- 50 D. Ke, H. Liu, T. Peng, X. Liu and K. Dai, Preparation and photocatalytic activity of WO₃/TiO₂ nanocomposite particles, *Mater. Lett.*, 2008, **62**, 447–450.
- 51 Y. Ding, T. A. J. Kuhlbusch, M. Van Tongeren, A. S. Jiménez, I. Tuinman, R. Chen, I. L. Alvarez, U. Mikolajczyk, C. Nickel, J. Meyer, H. Kaminski, W. Wohlleben, B. Stahlmecke, S. Clavaguera and M. Riediker, Airborne engineered nanomaterials in the workplace—a review of release and worker exposure during nanomaterial production and handling processes, *J. Hazard. Mater.*, 2017, **322**, 17–28.
- 52 J. Morin, A. Gandolfo, B. Temime-Roussel, R. Streckowski, G. Brochard, V. Bergé, S. Gligorovski and H. Wortham, Application of a mineral binder to reduce VOC emissions from indoor photocatalytic paints, *Build. Environ.*, 2019, **156**, 225–232.
- 53 A. Massari, M. Beggio, S. Hreglich, R. Marin and S. Zuin, Behavior of TiO₂ nanoparticles during incineration of solid paint waste: A lab-scale test, *Waste Manage.*, 2014, **34**, 1897–1907.
- 54 H. R. Paur, F. R. Cassee, J. Teeguarden, H. Fissan, S. Diabate, M. Aufderheide, W. G. Kreyling, O. Hänninen, G. Kasper, M. Riediker, B. Rothen-Rutishauser and O. Schmid, In-vitro cell exposure studies for the assessment of nanoparticle toxicity in the lung—A dialog between aerosol science and biology, *J. Aerosol Sci.*, 2011, **42**, 668–692.